# We are IntechOpen, the world's leading publisher of Open Access books Built by scientists, for scientists

**4,800**
Open access books available

**122,000**
International authors and editors

**135M**
Downloads

Our authors are among the

**154**
Countries delivered to

**TOP 1%**
most cited scientists

**12.2%**
Contributors from top 500 universities


WEB OF SCIENCE™

Selection of our books indexed in the Book Citation Index in Web of Science™ Core Collection (BKCI)

## Interested in publishing with us?
## Contact book.department@intechopen.com

Numbers displayed above are based on latest data collected.
For more information visit www.intechopen.com

9

# A Mutual Information-Based Image Quality Metric for Medical Imaging Systems

Du-Yih Tsai, Eri Matsuyama and Yongbum Lee
*Niigata University*
*Japan*

## 1. Introduction

Information on physical image quality of medical images is important for imaging system assessment in order to promote and stimulate the development of state-of-the-art imaging systems. In this chapter, we present a method for quantifying overall image quality of digital imaging systems using mutual information (MI) metric. The MI which is a concept from information theory is used as a measure to express the amount of information that an output image contains about an input object. The MI value is considered that it can be used to express combined physical properties of image noise, resolution and contrast of an imaging system. The higher the MI value, the better the image quality. The advantages of using the MI metric are: (1) simplicity of computation, (2) simplicity of experimentation, and (3) combined assessment of image contrast, noise and resolution.

The structure of this chapter is as follows. Section **.2 provides a basic overview of factors that affect medical image quality. Section **.3 describes the mutual information-based evaluation framework utilized in this work. An example of how to calculate MI is also given to provide a deep understanding of applying MI to the evaluation of medical imaging systems. Section **.4 shows a series of computer simulations, followed by investigating the utility and superiority of MI method by evaluating the performance of two imaging-plate detectors. Section **.5 presents the results that were obtained. Section **.6 ends with a discussion and conclusions.

## 2. Background

In medical imaging, image quality is determined by at least five factors: contrast, resolution, noise, artifacts, and distortion. Of these factors, resolution and noise are the most commonly used physical characteristics. As is well known, they are described by the modulation transfer function (MTF) and noise power spectrum (NPS), respectively. The MTF describes the ability of an imaging system to reproduce the frequency information contained in the incident x-ray signal. The NPS describes the frequency content of the noise of an imaging system. However, one of the dilemmas in medical radiography is the extent to which theses characteristics affect image quality. In comparison of two imaging systems, for example, an imaging system may only be superior in one physical characteristic while being inferior to another in the other characteristic. To deal with this issue, the noise equivalent quanta or detective quantum efficiency (DQE), which can be calculated if the MTF, NPS, and the input

signal-to-noise ratio of the x-ray beam used to measure the NPS are known, is used as a single parameter to describe the general quality of the system. Measurements of the MTF and NPS are conceptually straightforward but difficult to carry out experimentally and accurately. Moreover, the results of these measurements vary with the methods employed. Therefore, a simple and synthetic method for measuring image quality has been desirable.

In this chapter, we present a simple and straightforward method for synthetically evaluating digital radiographic images using MI. MI originating from information theory has been used as an effective similarity metric in medical image registration tasks and template matching schemes, and used as a feature selection criterion in computer-aided detection (Last et al., 2001; Pluim et al., 2003; Saunders et al., 2003; Tourassi et al., 2007). From the diversity of modalities (for example, computed tomography, magnetic resonance, and positron-emission tomography) and objects (the imaged anatomy) found in the literature, it is clear that MI has become a generally applicable measure. Here, the difference between the MI employed in image fusion and that employed in the present work needs to be clarified. In image fusion, MI is a similarity measure and usually serves as a criterion of alignment between two images. MI reaches its maximum value when two images are well aligned. In contrast, in the current work, MI is a physical measure of image quality and serves as a metric of overall physical quality of the imaging system being investigated. MI reaches its maximum value when the detected image (output of the transmission channel) completely corresponds to the image object (input of the transmitted channel).

Several studies have been published on the relation between MI and image quality. Using two Lucite step-wedges as phantoms to study the relations between MI and image noise as well as image blurring was made (Tsai et al., 2008) . However, the study did not examine the effect of image contrast on MI. Moreover, it did not make a comparison of MI with the MTF, NPS, and DQE. Investigating the combined effect of noise and resolution degradation on MI value by employing two imaging plates used for computed radiography was also conducted (Matsuyama et al., 2008). These pervious studies concluded that MI has close correlation with both image noise and image blurring. However, the study has not taken into account the effect of image contrast on MI. Furthermore, it did not make a direct comparison of MI with other image quality metric such as DQE.

The current study includes the following contents: (1) investigating individual and combined effects of contrast, noise and blur on images obtained from medical imaging systems; (2) conducting various simulation studies with a parametric model to verify the relationship of MI among the three major physical factors affecting image quality in medical imaging systems; and (3) comparing the evaluation results obtained using the MI metric to that using the DQE metric. In addition, two imaging plates for computed radiography were used for verification of the potential usefulness of the MI metric. The verification was made by showing clinical images with discussion.

## 3. Mutual information-based evaluation framework

MI is briefly described as follows.

Given events $S_1$,….. $S_n$ occurring with probabilities $p(S_1)$, …….$p(S_n)$, then the average uncertainty associated with each event is defined by the Shannon entropy as

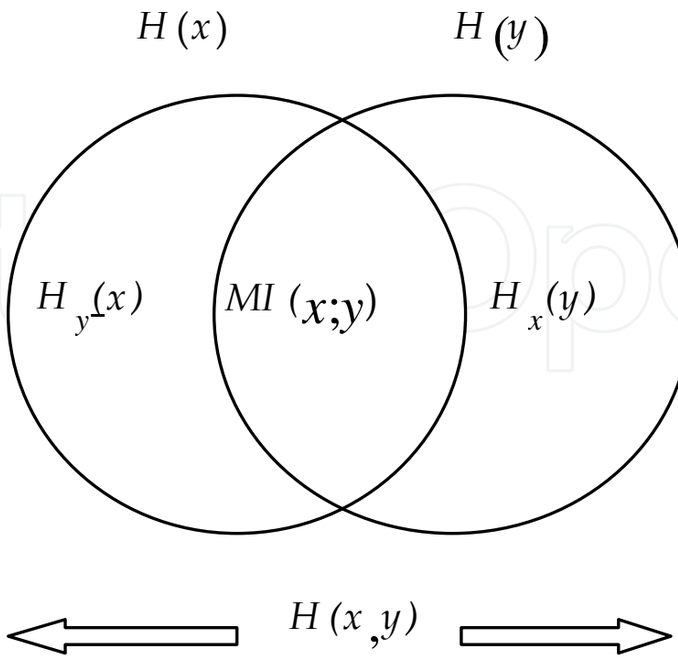


Fig. 1. Relationship among $H(x)$, $H(y)$, $H(x,y)$, $H_x(y)$, $H_y(x)$, and $MI(x;y)$.

$$H(S) = -\sum_{i=1}^{n} p(S_i) \cdot \log_2 p(S_i) \tag{1}$$

Considering $x$ and $y$ as two random variables corresponding to an input variable and an output variable, the entropy for the input and that for the output are denoted as $H(x)$ and $H(y)$, respectively. For this case the joint entropy, $H(x,y)$, is defined as

$$H(x,y) = H(x) + H_x(y) = H(y) + H_y(x) \tag{2}$$

where $H_x$(y) and $H_y(x)$ are conditional entropies. They are the entropy of the output when the input is known and that of the input when the output is known, respectively. In this situation, we can compute MI, $MI(x;y)$, as:

$$\begin{aligned} MI(x;y) &= H(x) - H_y(x) = H(y) - H_x(y) \\ &= H(x) + H(y) - H(x,y) \end{aligned} \tag{3}$$

A useful way of visualizing the relationship between these entropies is provided by a Venn diagram as shown in Fig.1. Consider an experiment in which every input has a unique output belonging to one of various output categories. In this study, for simplicity, the inputs may be considered to be a set of subjects (e.g., phantoms in simplicity) varying in composition, while the outputs may be their corresponding images varying in optical density or gray level. An orderly system is employed in the present study to calculate the entropies of input, output, and their joint entropies (Attneave, 1959). With this orderly system, the amount of MI is easily computed. The frequency with which each output is made to each input is recorded in Table 1.

| | Input $x$ | | | | | | |
|---|---|---|---|---|---|---|---|
| Output $y$ | $x_1$ | $x_2$ | ⋯ | $x_i$ | ⋯ | $X$ | Frequency |
| $y_1$ | $n_{11}$ | $n_{21}$ | ⋯ | $n_{i1}$ | ⋯ | $n_{X1}$ | $n_{j=1}$ |
| $y_2$ | $n_{12}$ | $n_{22}$ | ⋯ | $n_{i2}$ | ⋯ | $n_{X2}$ | $n_{j=2}$ |
| $y_3$ | $n_{13}$ | $n_{23}$ | ⋯ | $n_{i3}$ | ⋯ | $n_{X3}$ | $n_{j=3}$ |
| ⋯ | ⋯ | ⋯ | ⋯ | ⋯ | ⋯ | ⋯ | ⋯ |
| $y_j$ | $n_{1j}$ | $n_{2j}$ | ⋯ | $n_{ij}$ | ⋯ | $n_{Xj}$ | $n_{j=j}$ |
| ⋯ | ⋯ | ⋯ | ⋯ | ⋯ | ⋯ | ⋯ | ⋯ |
| $Y$ | $n_{1Y}$ | $n_{2Y}$ | ⋯ | $n_{iY}$ | ⋯ | $n_{XY}$ | $n_{j=Y}$ |
| Frequency | $n_{i=1}$ | $n_{i=2}$ | ⋯ | $n_{i=i}$ | ⋯ | $n_{i=X}$ | $n$ |

Table 1. A data matrix of occurrence frequency for Y outputs to X inputs.

The columns and lows of this table represent various inputs and outputs. The various inputs, $x_1$, $x_2$……$x_i$…..$X$, are assumed to take discrete values of input variables $x$. Likewise, the various outputs, $y_1$, $y_2$……$y_j$….$Y$ are discrete values of output variables $y$. The upper-case $X$ and $Y$ stand for the number of input and output categories, respectively. Note that the subscript $i$ refers to any particular but unspecified input, whereas the subscript $j$ refers to any particular but unspecified output. The number of times input $x_i$ is presented will be symbolized by $n_i$, the frequency of output, $y_j$, by $n_j$, and the frequency, with which the input $x_i$ corresponds to the output $y_j$, is given by $n_{ij}$. The total of all frequencies is given by $n$. It is apparent from Table 1 that

$$\sum_j n_{ij} = n_i \tag{4}$$

$$\sum_i n_{ij} = n_j \tag{5}$$

$$\sum_{ij} n_{ij} = \sum_i n_i = \sum_j n_j = n \quad . \tag{6}$$

Referring to the definition of information entropy as shown in Equation (1), three informational quantities, namely, $H(x)$, $H(y)$, and $H(x,y)$, can be calculated from Table 1.

$$H(x) = \sum_i p_i \log_2(1/p_i) \tag{7}$$

$$H(y) = \sum_j p_j \log_2(1/p_j) \tag{8}$$

$$H(x,y) = \sum_{ij} p_{ij} \log_2 (1 / p_{ij}) \tag{9}$$

where $p_i = n_i / n$, $p_j = n_j / n$, and $p_{ij} = n_{ij} / n$. For simplicity, we can rewrite the above equations as follows:

$$H(x) = \log_2 n - (1/n) \sum_i n_i \log_2 n_i \tag{10}$$

$$H(y) = \log_2 n - (1/n) \sum_j n_j \log_2 n_j \tag{11}$$

$$H(x,y) = \log_2 n - (1/n) \sum_{ij} n_{ij} \log_2 n_{ij} \tag{12}$$

Then, the MI $MI(x;y)$ can be obtained from Equation (3) together with Equations (10), (11), and (12). The MI conveys the amount of information that "$y$" has about "$x$".

Table 2 gives an example of how to calculate MI. Assume that a subject (e.g., a step-wedge) having five steps with different thickness was used for the experiment. The five steps correspond to five inputs present equiprobably. The gray-scale pixel values of 100 pixels in each step after imaging were measured randomly. The distributions of the pixel values are considered as the corresponding outputs and their respective frequencies are given in the table. The frequencies will be referred to by means of the symbols given in Table 1; for example: $n_{12}$=60, $n_{j=3}$=118, $n_{i=2}$=100, $n$=500, and so on. Now, there are three information quantities, namely, $H(x)$, $H(y)$, and $H(x,y)$, that can be calculated directly from Table 2 by using equations (10), (11), and (12).

| | Input x | | | | | |
|---|---|---|---|---|---|---|
| Output y | 1 | 2 | 3 | 4 | 5 | Frequency |
| 1 | 20 | | | | | 20 |
| 2 | 60 | 4 | | | | 64 |
| 3 | 20 | 88 | 10 | | | 118 |
| 4 | | 8 | 76 | 14 | | 98 |
| 5 | | | 12 | 80 | 2 | 94 |
| 6 | | | 2 | 6 | 8 | 16 |
| 7 | | | | | 90 | 90 |
| Frequency | 100 | 100 | 100 | 100 | 100 | 500 |

Table 2. An example of how to calculate the mutual information. The frequencies shown in the table is referred to by means of the symbols given in Table 1, for example, $n_{23}$=88, $n_{j=2}$=64, $n_{i=1}$=100, $n$=500, and so on.

For the data given in Table 2,

$$H(x) = \log_2 n - (1/n)\sum_i n_i \log_2 n = \log_2 5 = 2.323 \quad \text{(since inputs are equiprobable)}$$

$$H(y) = \log_2 500 - (1/500) \times (20\log_2 20 + 64\log_2 64 + 118\log_2 118 .....etc.) = 2.575$$

$$H(x,y) = \log_2 500 - (1/500) \times (20\log_2 20 + 60\log_2 60 + 4\log_2 4 .....etc.) = 3.235$$

Applying Equation (3) to the values calculated above, we have

$$MI(x;y) = H(x) + H(y) - H(x,y) = 2.323 + 2.575 - 3.235 = 1.663 .$$

This is the estimate of the amount of information transmitted by the subject from input to output: 1.633 bits, out of a possible of 2.323 bits.

If the output is identical to the input, then knowing the output provides complete information about the input. In this case, the MI is maximized and equal to the input entropy, and the uncertainty of the input is reduced to 0. It means that knowing (or viewing) the image of an object (subject) receives complete information about the object (subject). Thus the quality of the obtained image reaches to a maximum in terms of the MI. If, on the other hand, the output and the input are independent, then knowing the output does not help make any conclusions about the input. In this case, MI value is zero, and therefore the uncertainty about the input remains unchanged. This means that the obtained image has the lowest quality from the point of view of the MI.

## 4. Materials and methods

### 4.1 Image simulation

Simulation studies were designed, and the framework is as follows. In mathematical terms, a simulated image $g(x,y)$ is the convolution of a uniformly distributed signal (an object) $f(x,y)$ and the blurring function $B$. If the noise $u(x,y)$ is also taken into consideration, the simulated image may be represented by the following formula:

$$g(x,y) = \sum_{k=1}^{5} \{[k \times f(x,y)] * B + u(x,y) \times W\} \tag{13}$$

where the symbol * represents the convolution operation, and $k$ is an integer representing the number of steps of the simulated image ($k$=1,2, ….5). In the simulation studies, the input signal is a five-step wedge or a five-gray-level grid pattern with a specific intensity or pixel value on each step. The term of $W$ is a weighting coefficient used to adjust the extent of noise, and $u(x,y)$ is a zero-mean Gaussian noise with a standard deviation of 0.5.

An image of a simulated step-wedge generated by using Equation (13) is shown in Fig.2(a). Five regions of interests (ROIs) indicated with rectangles near the boundaries of two adjacent steps were chosen for calculation of MI. The five steps of the image are numbered from the right as step 1, step 2, and so on. The left band without a rectangular box is considered as the background of the image. The corresponding pixel-value distributions measured from the ROIs are given in Fig.2(b). The area of each ROI used in this study was

50×200 pixels. As a result, a total of 10,000 data for each step was obtained. As shown in Fig.2(a), the number of inputs is five, and the number of outputs is the range of gray levels shown on the horizontal axis of the pixel-value distributions [see Fig.2(b)].

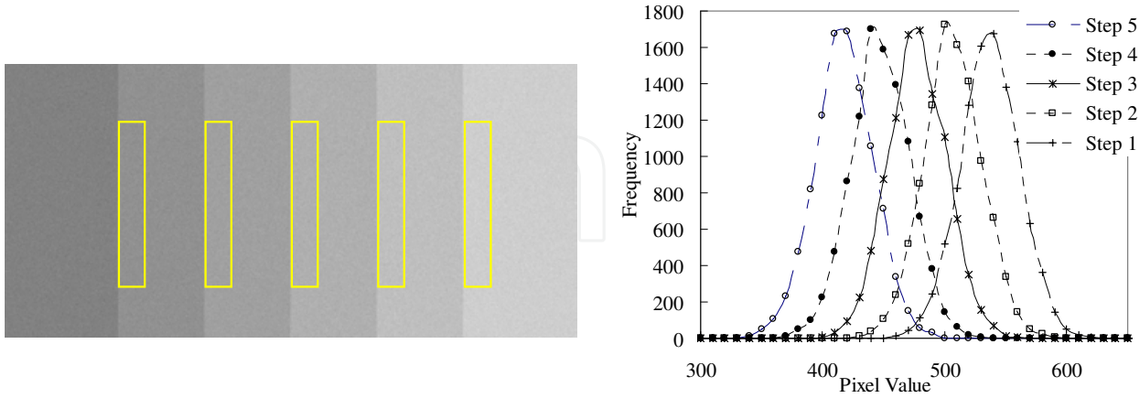


(a) (b)

Fig. 2. (a) Computer-simulated step-wedge. A region of interest (ROI) shown with a rectangle at each step of the step-wedge was chosen for entropy computation. (b) The corresponding pixel-value distributions measured from the ROIs shown in (a).

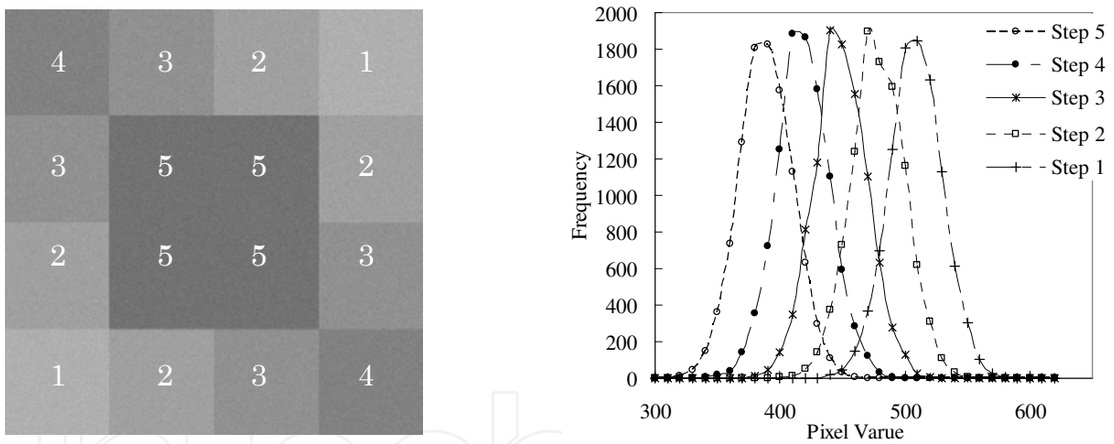


(a) (b)

Fig. 3. (a) Simulated grid-pattern image with five different gray levels. (b) The corresponding pixel-value distributions measured from the ROIs of (a).

Grid-pattern images with various noise levels and different size of blur were also generated using Equation (13) for another simulation study. A simulated grid-pattern image is illustrated in Fig.3(a). Five different gray levels were used to construct the grid-pattern image. The image consists of 16 blocks and is symmetric with respect to the main diagonal. An ROI with a size of 50×50 was selected from the central area of the blocks numbered 2, 3, and 5, while two nonoverlapped ROIs near the central area of the blocks numbered 1 and 4 (at the four corners) were chosen for MI measurement. As a result, a total of 10,000 data for a specific gray level could be obtained. Fig.3(b) illustrates the corresponding pixel-value distributions measured from the ROIs of the simulated image [Fig.3(a)].

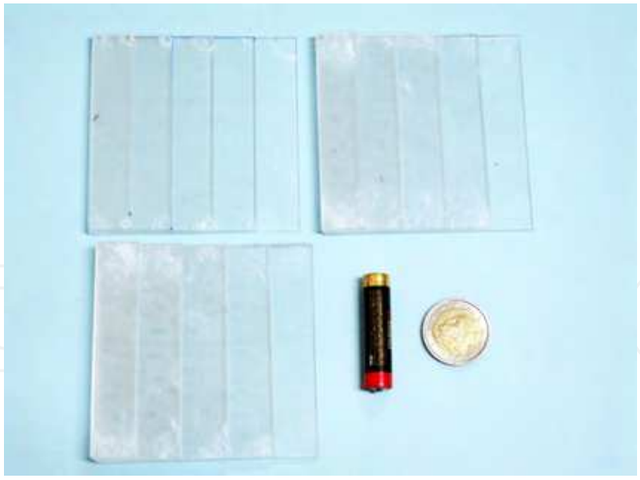

Fig. 4. Photograph of the three step-wedges (phantoms A, B, and C) used in the experiments.

Three different simulations were performed using the simulated step-wedge and grid pattern. The first simulation was carried out to investigate the relationship between image contrast and MI for various noise levels and different extent of blurring. In this study, we defined image contrast as the difference of the mean pixel values between two adjacent steps of a simulated step-wedge [Fig.2(a)] or the difference between two consecutive numbers of gray-level steps [Fig.3(a)]. We employed signal-to-noise ratio (SNR) to describe the extent of noise level. The signal and noise used for SNR calculation were $f(x,y)$ and $u(x,y)\times W$, respectively, as given in Equation (13). As a blurring function, we used a Gaussian filter with a size of $d\times d$ ($d$ is an odd integer). The extent of blurring was adjusted by varying the filter size. The second simulation was performed to investigate the relationship between the image noise and MI for different extent of blurring and various levels of contrast. The third simulation was conducted to investigate the relationship between the blurring and MI for various levels of noise and contrast.

### 4.2 Real images of step wedges

In addition to the simulation studies, phantom studies were also conducted (Matsuyama et al., 2009). Three Lucite step-wedges with 0, 0.5, 1.0, 1.5, 2.0, and 2.5 mm (phantom A); 0, 1, 2, 3, 4, and 5 mm (phantom B); and 0, 1.5, 3.0, 4.5, 6.0, and 7.5 mm (phantom C) in thickness were used as objects for experiments (see Fig.4). Two imaging plates (IPs) for computed radiography (standard resolution type ST and high resolution type HR, Fuji Film Inc., Tokyo, Japan) were used as detectors to record x-ray intensities for performance evaluation. It is known that the intensity of the transmitted x-ray beam is reduced when the thickness of the step-wedge increases. The area of each ROI and the number of data used for calculation of MI were the same as those used in the step-wedge simulation studies.

### 4.3 Detective quantum efficiency measurement

In order to connect MI to the commonly used image quality metric, the DQE that is usually obtained from presampling MTF and NPS was measured. As is well known, the presampling MTF and NPS are used to describe the spatial resolution properties (blur) and

noise properties of imaging systems, respectively. The presampling MTF of IPs was measured with an angled-edge method (Samei et al., 1998). The edge is made of a 100-μm-thick sharp-edged-tungsten plate, and its dimension was 10×10 cm². After the image of the edge was acquired, the digital image data were transferred to a computer for computation. The details of the processing method are given elsewhere (Flymn & Samei, 1999). NPS measurements were made by exposing IPs to a uniform beam of radiation. For the calculation, the central portion of each obtained uniform image was divided into multiple non-overlapping regions, 256×256 in size. A total of 25 regions were used. The details of the methodology are reported elsewhere (Monnin et al., 2007; Samei & Flynn, 2002).

The DQE is a spatial frequency-based measurement of the ability of the imaging device to convert the spatial information contained in the incident x-ray fluence to useful image information (Fetterly & Hangiandreou, 2001; Neitzel et al., 2004; Spahn, 2005). It is defined as

$$DQE = SNR^2_{out} \,/\, SNR^2_{in} \tag{14}$$

where $SNR_{out}$ and $SNR_{in}$ are the spatial frequency-dependent signal-to-noise ratios of the imaging device at the output and input, respectively. It was calculated using the following formula (Fettery & Schueler, 2006).

$$DQE = MTF^2 \,/\, (q \times NNPS) \tag{15}$$

where $q$ is the x-ray photon fluence density ($mm^{-2}$) used for the uniform exposure image, and $NNPS$ is the normalized $NPS$. For a perfect imaging detector, DQE can reach a maximum value of 1.0.

As can be seen from Equation (15), three quantities must be measured to obtain DQE. It is obvious from the equation that DQE value would be high when any of the following situations occurs: (1) high MTF value (high spatial resolution), (2) low NNPS value ( low noise level), and (3) low x-ray photon fluence density. Because the calculation of DQE includes a complicated set of measurements, there is thus a need to provide an easier and less complicated methodology for the use of assessing overall image quality. The present work was just motivated by this need.

## 5. Results

Simulations were performed to investigate individual effects of contrast, noise and blur on MI. Fig.5(a) shows the relationship between the contrast and MI for different levels of SNR, when the filter size (FS) of blurring function was 1×1 (FS=1). On the left is the result obtained from the simulated step-wedges, while on the right is that obtained from the simulated grid patterns. Fig.5(b) illustrates the relationship between the contrast and MI for various levels of blur, when the SNR was fixed at 35 dB.

As a whole, the results show that MI increases with the increase of image contrast at constant levels of noise and blur. It is seen from Fig.5(a) that the MI at low noise levels (high level of SNR) shows remarkable increase as compared to high noise levels (low level of SNR). For example, the MI value at SNR of 31 is considerably lower than that at SNR of 40.

This means that the MI value is greatly influenced by the noise level. As shown in Fig.5(b), the MI curves of different levels of blur (filter size; FS) are similar in shape. The difference in MI values at low contrast level is not obvious, even if the filter sizes change. However, the difference becomes notable at high contrast levels. The results demonstrate that the effect of blur on MI value is more obvious at higher contrast levels as compared to that at lower contrast levels. It is noted that the results obtained by using the simulated step-wedges and that by the grid patterns have a similar tendency.

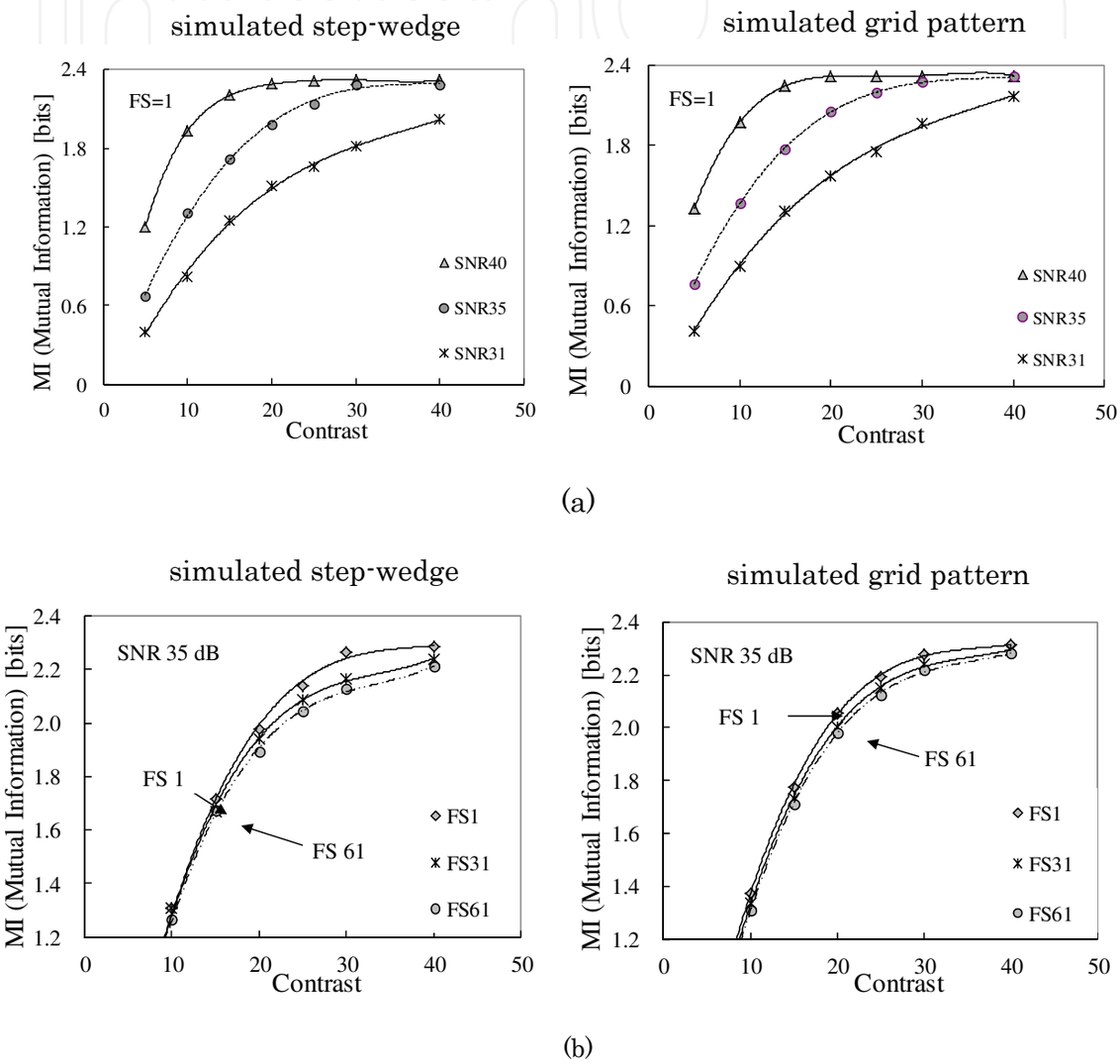


Fig. 5. Relationship between the contrast and MI. Left column: simulated step-wedge. Right column: simulated grid pattern. (a) For various levels of SNR at a size of blurring function FS of 1. (b) For various levels of blur at an SNR of 35dB.

Figs.6(a) and 6(b) illustrate MI as a function of SNR for various levels of blurring at image contrast of 20 and for different contrast levels at FS=1, respectively. The results from the figures indicate that the MI value increases with the increase of SNR (decrease in noise

level). The figures on the left were the results from the simulated step-wedges, while those on the right were from the simulated grid patterns. It is seen from Fig.6(a) that the difference in MI values among various filter sizes at low SNR levels (high noise levels) is not significant. Similar results were obtained at high SNR levels (low noise levels). MI reaches to its maximum when SNR is higher than 45 dB. This implies that MI could be almost the same value when noise level is lower than a certain level. As illustrated in Fig.6(b), the MI curves for different contrast levels are in similar shape. MI reaches to the maximum when SNR is approximately 38 dB at contrast of 30, and similarly, when SNR is 40 dB at contrast of 20. This means that the two images would provide the same image quality in terms of MI metric. It is noted that the results obtained from the simulated step-wedge and those from grid patterns have the same tendency.

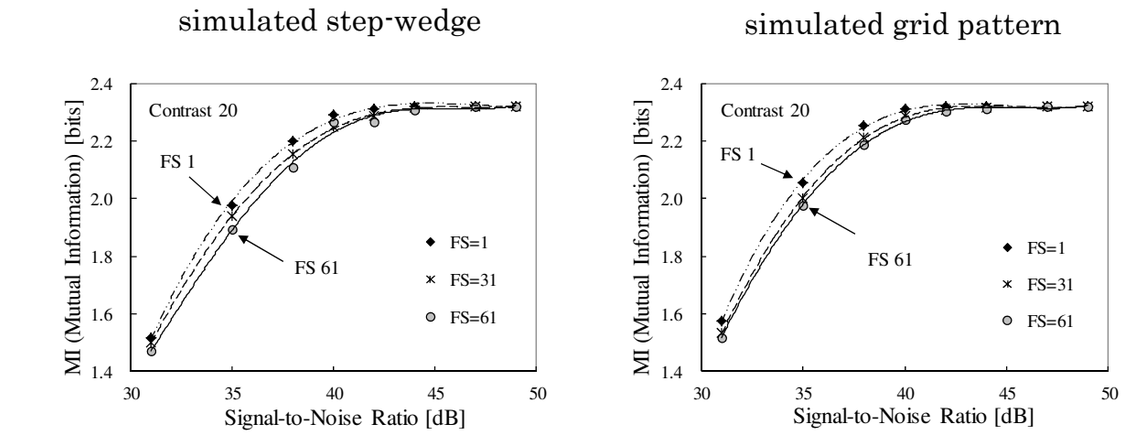


Fig. 6. Relationship between the SNR and the MI. Left column: simulated step-wedge. Right column: simulated grid pattern. (a) For various levels of blur at an image contrast of 20. (b) For various levels of contrast at a size of blurring function (FS) of 1.

Fig.7(a) shows MI as a function of filter size of blurring function for various levels of SNR at image contrast of 20 for the simulated step-wedges (left) and grid patterns (right). Fig.7(b) shows MI as a function of filter size of blurring function for various contrast levels at SNR of 35 dB for the two various simulated images. The results from the figures show that MI value decreases when filter size of the blurring function increases, although the decrease is relatively small. This means that the effect of the level of blur on the MI is not so obvious in comparison to noise and contrast. Fig.8 illustrates images of the simulated step-wedges and grid patterns with different sizes of blurring (FS=7, 21, and 41), while the SNR and image contrast were kept constant at 30 and 20, respectively. The images demonstrate that image resolution degrades with the increase of filter size of blurring function. Therefore, MI values decrease with the increase of filter size.

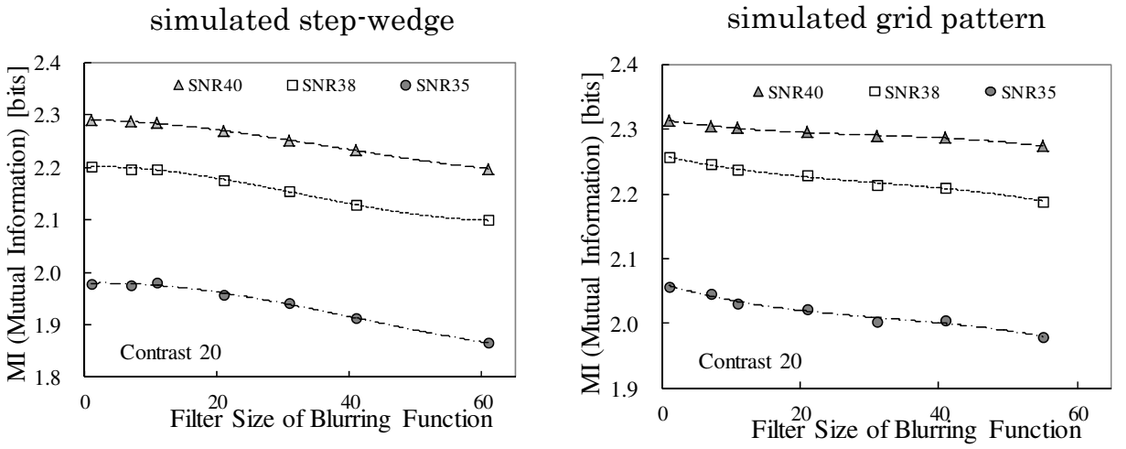


Fig. 7. Relationship between the filter size of blurring function and the MI. Left column: simulated step-wedge. Right column: simulated grid pattern. (a) For various levels of SNR at an image contrast of 20. (b) For various levels of image contrast at a SNR of 35 dB.

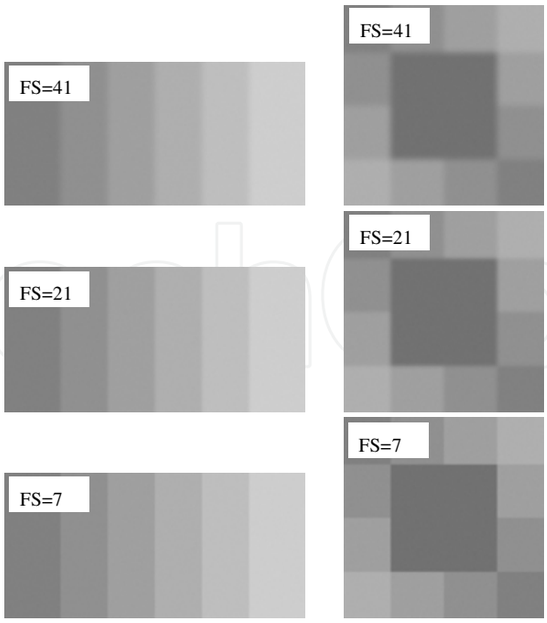


Fig. 8. Images of the simulated step-wedge and grid pattern with different sizes of blurring (FS=7, 21, and 41), while the SNR and image contrast were kept constant at 30 and 20, respectively.

Fig.9 shows MI as a function of exposure dose for the images of a Lucite step-wedge (phantom B) obtained with ST and HR IPs for computed radiography. The results illustrate that MI increases with the increase of exposure dose. The rise of MI value might be mainly due to the decrease of noise, resulting from the increase of radiation dose. The trend of the

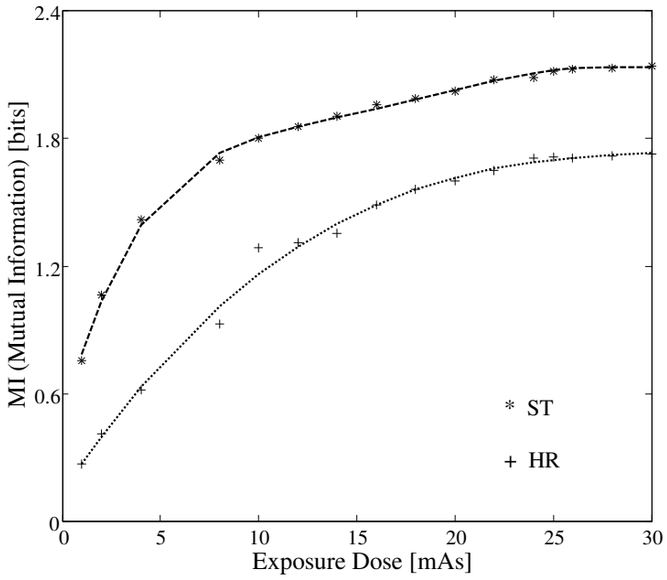


Fig. 9. Mutual information as a function of exposure dose for the images of a Lucite step-wedge (phantom B) obtained with ST and HR imaging plates.

MI curves is similar to that shown in Fig.6(b), although the two figures are plotted with different units: one is the exposure dose, and the other is the SNR. However, it is reasonable to say that the two units are associated with noise levels and are closely correlated. As shown in the figure, the MI value for the ST plate is higher than that for the HR plate at the same exposure dose. This can be explained by the fact that combined effects of blur and noise lead to a higher MI value for the ST plate at a given image contrast. This suggests that the image obtained with the ST plate transmits more information in comparison to that with the HR plate under the same exposure conditions.

Fig.10(a) illustrates the measured presampling MTFs of the two IPs at 42 kV. The result indicates that the HR plate has higher MTF as compared to the ST plate. This is mainly due to the difference in the spatial resolution of the two IPs: HR is a high-resolution plate, while ST is a standard one.

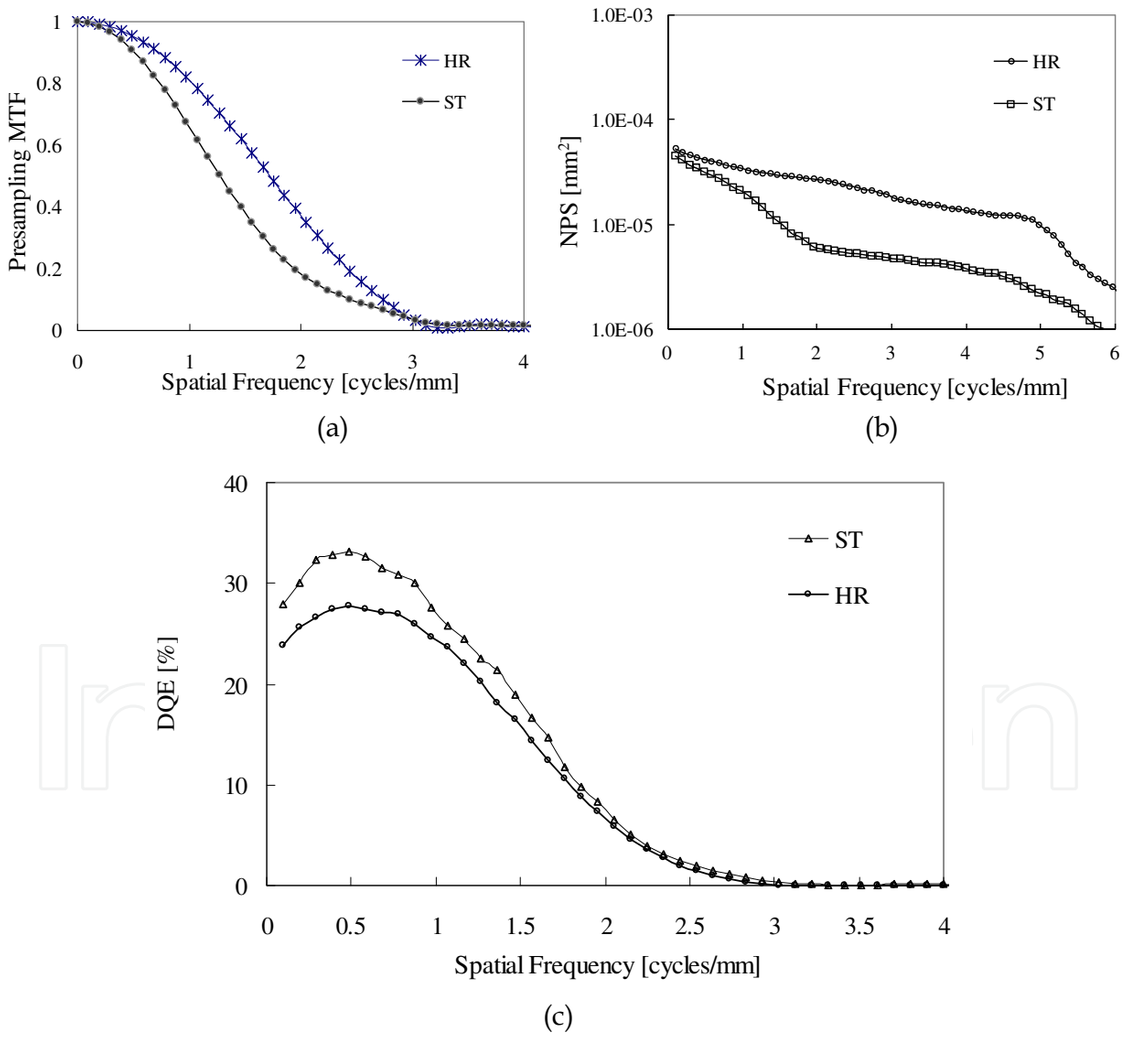


Fig. 10. (a) Experimental results for the presampling MTF measurement with the edge method for the two imaging plates. (b) NPS versus spatial frequency for the two imaging plates. (c) DQE versus spatial frequency at 76-μGy exposure level for the two imaging plates.

In Figs.11 and 12, we display the real images of the femur and metacarpus acquired with ST and HR IPs under the same exposure conditions. In these two figures, the left column illustrates the original images, while on the right are the magnified images of the white squares indicated in the original images. It is clear from the magnified images of Fig.11 that the lesser trochanter (with a white arrow) obtained with HR plate shows better resolution as compared to ST plate. Similarly, the magnified images of Fig.12 (the carpal bone indicated by white arrows) obtained with HR plate shows better resolution as compared to ST plate. The experimental validation provides confirming evidence for the MTF results.

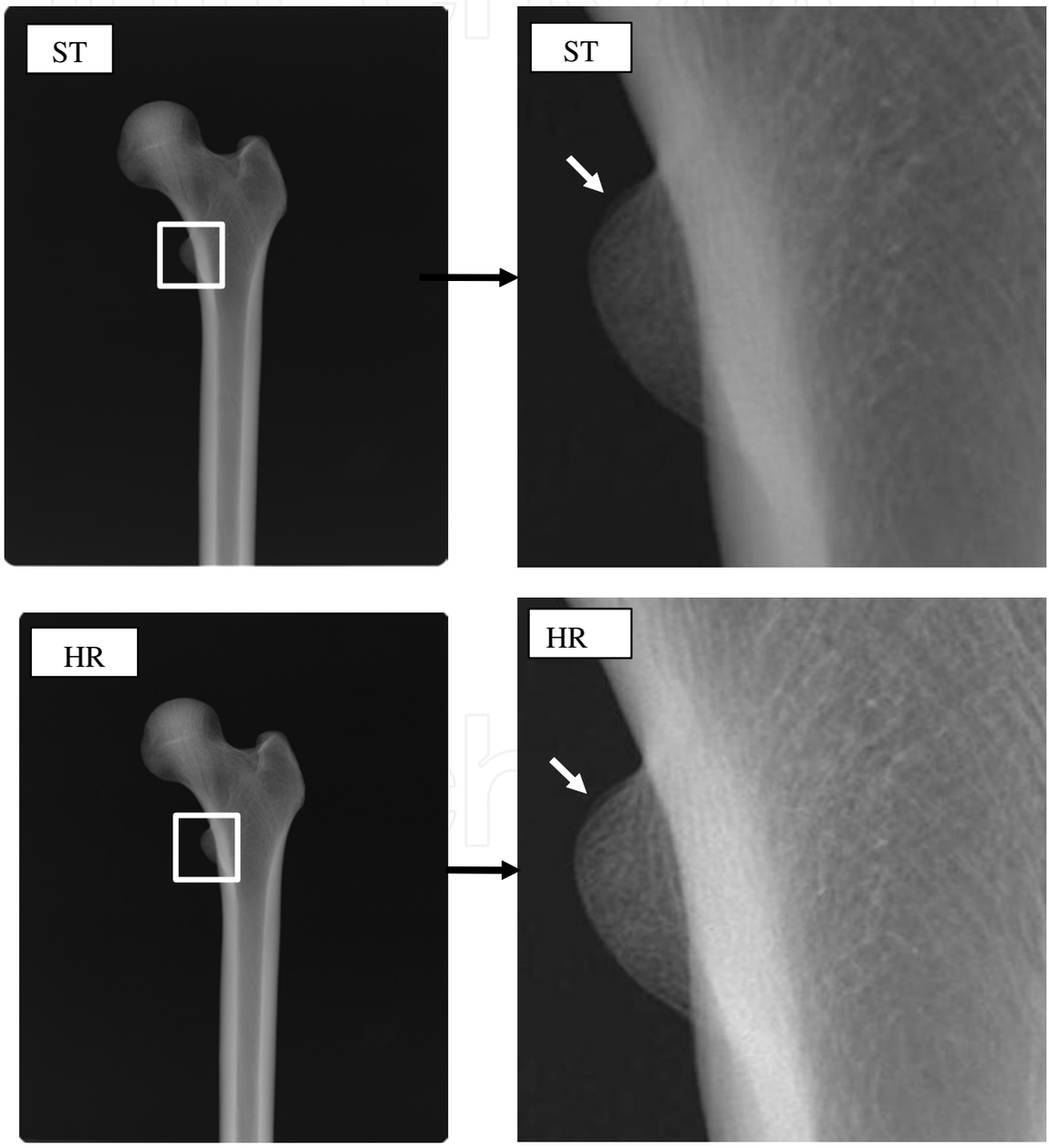


Fig. 11. Clinical images of the femur acquired with ST and HR image plates.

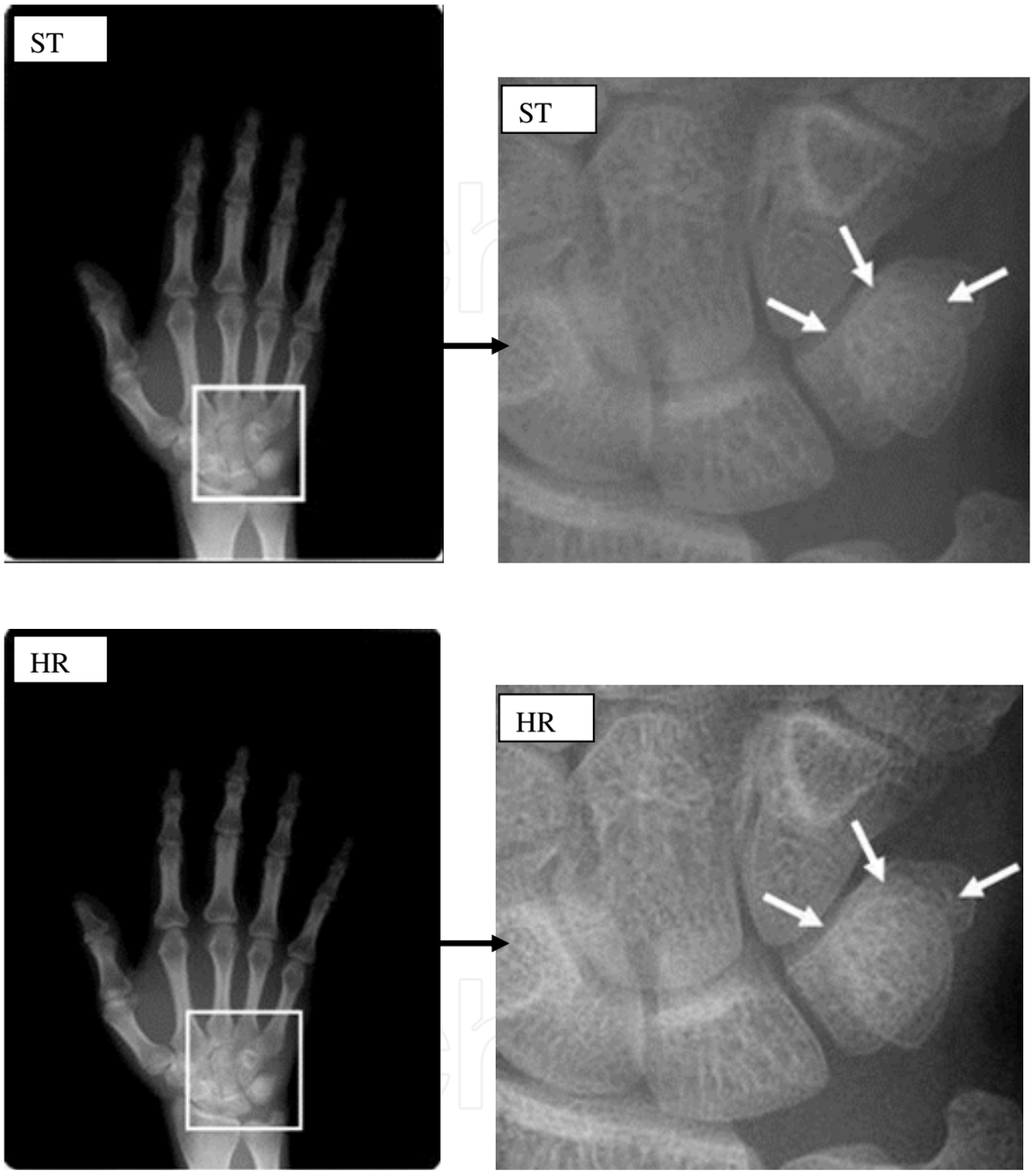


Fig. 12. Clinical images of the metacarpus acquired with ST and HR image plates.

Fig.10(b) illustrates the NPS versus spatial frequency at 42 kV acquired with ST and HR IPs. As shown in the figure, the NPS of the HR IP is higher than that of the ST plate at the same radiation dose. It can be seen from the magnified images of Figs.11 and 12 that the images acquired with HR plates show higher noise levels. The perceptual results correctly reflect the outcome of the NPS shown in Fig.10(b).

The DQEs of ST and HR IPs versus spatial frequency at 76-μGy exposure level are presented in Fig.10(c). In the present study, the DQEs were assessed using Equation (15) — in order words, the results of Fig.10(c) were obtained from the measured results shown in Figs.10(a) and 10(b). It is known that the MTF values are generally independent of exposure levels. Thus the MTF values shown in Fig.10(a) were used for calculating the DQEs of IPs at different exposure doses. In spite of having lower MTFs, the DQEs for the ST plates are higher than those for the HR plates at the same exposure level. The higher value in DQE might be attributed to the better noise performance of ST plates. In other words, as compared to resolution, noise greatly affects overall performance of the imaging systems.

When looking at Fig.9 and Fig.10(c), the performance ranking of MI values for ST and HR IPs and those of DQE values for the two IPs are the same, *i.e.*, the MI value and DQE value for the ST plate are higher than those for the HR plate. The experimental results may confirm that MI and DQE metrics are highly correlated.

## 6. Discussion and conclusions

In our simulation studies, we demonstrated that MI increases with the increase of contrast and decreases with the increase of noise and blur. Therefore, it is considered that MI could be used as a simple metric for evaluation of overall imaging performance. In this study, we applied the MI metrology to evaluate the performance of two IPs for computed radiography. The measured MI shown in Fig.9 is consistent with the DQE shown in Fig.10(c), although they are described in different domains: one is in the spatial domain scalar metric, and the other is in the spatial frequency domain metric. The results suggest the usefulness of the proposed MI metric.

There are several advantages of using the MI metric to evaluate the performance of imaging systems. First, computation of MI is much easier in comparison to that of spatial frequency domain measures such as MTF, NPS and DQE. Second, the experiment setup is simple. For example, a step-wedge or an equivalent test device is sufficient for conducting experiments. Third, three of the most important image quality factors, *i.e.*, contrast, noise, and blur, can be integrated for overall evaluation. However, it should be stated clearly that our proposed MI metric is not intended for replacing the conventionally used metrics. The main objective of the present work is to provide a scalar metrology based on simple image statistics for image quality evaluation.

In conclusion, we have described an information-theoretic method for quantifying overall image quality in terms of MI. We demonstrated by way of image simulation that MI increases with contrast, decreases with noise, and increases with resolution. We investigated the utility of this method by applying it to evaluating the performance of two imaging detectors. We also compared evaluation results in terms of MI against those in terms of the commonly used DQE metric. Our simulation and experimental results demonstrate that the proposed method is simple to implement and has potential usefulness for evaluation of overall image quality.

## 7. Acknowledgment

This work was supported in part by the Ministry of Education, Culture, Sports, Science and Technology of Japan (Tokyo, Japan) through a grant-aid for Scientific Research (23602004).

## 8. References


Attneave, F. (1959). *Applications of Information Theory to Psychology.* Holt, Rinehart and Winston, New York

Fetterly, K.A. & Hangiandreou, N.J. (2001). Effect of x-ray spectra on the DQE of a computed radiography system. *Medical Physics,* Vol.28, pp. (241-249)

Fettery, K.A. & Schueler, B.A. (2006). Performance evaluation of a computed radiography imaging device using a typical front side and novel dual side readout storage phosphors. *Medical Physics.* Vol.33, pp. (290-296)

Flynn, M. & Samei, E. (1999). Experimental comparison of noise and resolution for 2k and 4k storage phosphor radiography systems. *Medical Physics,* Vol.26, pp. (1612-1623)

Last, M.; Kandel, A. & Maimon, O. (2001). Information-theoretic algorithm for feature selection. *Pattern Recognition Letters,* Vol.22, pp. (799-811)

Matsuyama, E.; Tsai, D.Y. & Lee, Y. (2009). Mutual information-based evaluation of image quality with its preliminary application to assessment of medical imaging systems. *Journal of Electronic Imaging*, Vol.18, pp. (033011-1-11)

Matsuyama, E.; Tsai, D.Y.; Lee, Y.; Sekiya, M. & Kojima, K. (2008). Physical characterization of digital radiological images by use of transmitted information metric. *Proceedings of SPIE Medical Imaging,* Vol.6913, pp. (69130V1-8)

Monnin, P.; Gutierrez, D.; Bulling, S.; Guntern, D. & Verdun, F.R. (2007). A comparison of the performance of digital mammography systems. *Medical Physics,* Vol.34, pp. (906-914)

Neitzel, U.; Gunther-Kohfahl, S.; Borasi, E. & Samei, E. (2004). Determination of the detective quantum efficiency of a digital x-ray detector: comparison of three evaluations using a common image data set. *Medical Physics,* Vol.31, pp. (2205-2211)

Pluim, J.P.M.; Maintz, J.M.A. & Viergever, M.A. (2003). Mutual-information-based registration of medical images: A survey. *IEEE Transactions on Medical Imaging,* Vol.22, pp. (986-1004)

Samei, E. & Flynn, M.J. (2002). An experimental comparison of detector performance for computed radiography systems. *Medical Physics,* Vol.29, pp. (447-459)

Samei, E.; Flynn, J. & Reimann, D.A. (1998). A method for measuring the presampled MTF of digital radiographic systems using an edge test device. *Medical Physics,* Vol.25, pp. (102-113)

Saunders, Jr R.S. & Samei, E. (2003). A method for modifying the image quality parameters of digital radiographic images. *Medical Physics,* Vol.30, pp. (3006-3017)

Spahn, M. (2005). Flat detectors and their clinical applications. *European Radiology,* Vol.15, pp(1934-1947)

Tourassi, G.D.; Harrawood, B.; Singh, S. & Lo, J.Y. (2007). Information-theoretic CAD system in mammography: Entropy-based indexing for computational efficiency and robust performance. *Medical Physics,* Vol.34, pp. (3193-3204)

Tsai, D.Y,; Lee, Y. & Matsuyama, E. (2008). Information-entropy measure for evaluation of image. *Journal of Digital Imaging,* Vol.21, pp. (338-347)

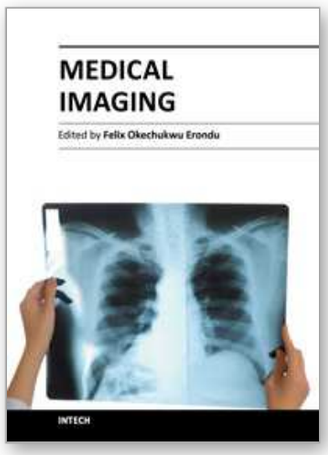


**Medical Imaging**

Edited by Dr. Okechukwu Felix Erondu

ISBN 978-953-307-774-1
Hard cover, 412 pages
**Publisher** InTech
**Published online** 22, December, 2011
**Published in print edition** December, 2011

What we know about and do with medical imaging has changed rapidly during the past decade, beginning with the basics, following with the breakthroughs, and moving on to the abstract. This book demonstrates the wider horizon that has become the mainstay of medical imaging sciences; capturing the concept of medical diagnosis, digital information management and research. It is an invaluable tool for radiologists and imaging specialists, physicists and researchers interested in various aspects of imaging.

**How to reference**

In order to correctly reference this scholarly work, feel free to copy and paste the following:

Du-Yih Tsai, Eri Matsuyama and Yongbum Lee (2011). A Mutual Information-Based Image Quality Metric for Medical Imaging Systems, Medical Imaging, Dr. Okechukwu Felix Erondu (Ed.), ISBN: 978-953-307-774-1, InTech, Available from: http://www.intechopen.com/books/medical-imaging/a-mutual-information-based-image-quality-metric-for-medical-imaging-systems

INTECH
open science | open minds

**InTech Europe**
University Campus STeP Ri
Slavka Krautzeka 83/A
51000 Rijeka, Croatia
Phone: +385 (51) 770 447
Fax: +385 (51) 686 166
www.intechopen.com

**InTech China**
Unit 405, Office Block, Hotel Equatorial Shanghai
No.65, Yan An Road (West), Shanghai, 200040, China
中国上海市延安西路65号上海国际贵都大饭店办公楼405单元
Phone: +86-21-62489820
Fax: +86-21-62489821

IntechOpen